

Generalizable task representation learning from human demonstration videos: a geometric approach

Jun Jin[†] and Martin Jagersand[†]

Abstract—We study the problem of generalizable task learning from human demonstration videos without extra training on the robot or pre-recorded robot motions. Given a set of human demonstration videos showing a task with different objects/tools (categorical objects), we aim to learn a representation of visual observation that generalizes to categorical objects and enables efficient controller design. We propose to introduce a geometric task structure to the representation learning problem that geometrically encodes the task specification from human demonstration videos, and that enables generalization by building *task specification correspondence* between categorical objects. Specifically, we propose CoVGS-IL, which uses a graph-structured task function to learn task representations under structural constraints. Our method enables task generalization by selecting geometric features from different objects whose inner connection relationships define the same task in geometric constraints. The learned task representation is then transferred to a robot controller using uncalibrated visual servoing (UVS); thus, the need for extra robot training or pre-recorded robot motions is removed.

I. INTRODUCTION

One interesting phenomenon in human learning by watching demonstrations is that we can not only infer the task definition (specification) from one demonstration video, but also generalize the same task specification by watching a collection of demonstration videos showing the same task using various objects or tools. In the low level, each video in the collection individually encodes a realization of the task with a specific object or tool demonstrated. In the high level, each video encodes a task specification that is the same to each other since the same task is defined. Therefore, there is a *task specification correspondence* between each demonstration video of the collection since the same task specification builds correspondence between task settings using different objects. Can we apply the same learning mechanism in robotics to enable generalizable task learning?

This problem is challenging in two folds. (1) First, if we put aside task generalization, the problem of robot learning by watching human demonstrations [1–6] is difficult since we only have video samples without any clues about robot actions. Enabling a robot to perform the task will require either tedious robot training [1, 2] or pre-recorded motions [3, 4], which impede its viability in the real world. (2) Learning generalizable skills from a collection of human demonstration videos remains an unsolved problem. Questions regarding what should be learned to achieve task generalization and why the learned model is generalizable

[†]Authors are with the Department of Computing Science, University of Alberta, Edmonton AB., Canada, T6G 2E8. {jjjin5,mj7}@ualberta.ca

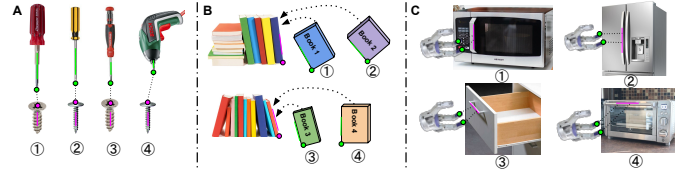


Fig. 1: Task specification correspondence and examples of using geometric task structures to specify a manipulation task (A: a screwing task. B: a book organization task. C: a door, drawer open task). For different objects/tools, the same type of geometric constraints (such as in Fig. 1A, point-to-point and line-to-line) defines the same task (screwing), which we call as *task specification correspondence* since the same task definition builds correspondence between task settings using different objects. Can we use this clue for generalizable task learning?

lack sufficient research attention. For example, should we enable generalization in the representation learning level or the policy learning level that maps observation to robot actions? Furthermore, suppose we can learn a generalizable representation or policy using deep neural networks, it remains challenging to interpret what has been learned to enable task generalization.

To address the above problems, we introduce a geometric task structure to learn generalizable representations from human demonstration videos. Commonly, there are two types of task structures: (1) a geometric task structure that uses geometric features (points, lines, planes) to compose projective-invariant constraints (point-to-point, parallel lines) to define a task; (2) a semantic task structure [7] that extracts task semantic meanings in the form of knowledge graphs [8], grammar trees [9], behaviour trees [10] or the planning domain definition language (PDDL) [11]. We choose a geometric task structure as the inductive bias in learning since its adjoint outputs—geometric errors, compared to a semantic task structure’s output, are more friendly to robot controllers as shown in the visual servoing literature [12]. As a result, it is likely to remove the requirement for tedious robot training or pre-recorded motions.

We show that introducing a geometric structure in learning also brings task generalization by building *task-specification correspondence* (Fig. 1), which means the task definition stays consistent under various task settings, such as different tools, objects or backgrounds. As a result, the consistency of task specification builds correspondence between different task settings, which is the key to achieve task generalization.

Specifically, we show that a geometric task structure can be used to build *task-specification correspondence* since the same type of geometric constraints defines the same

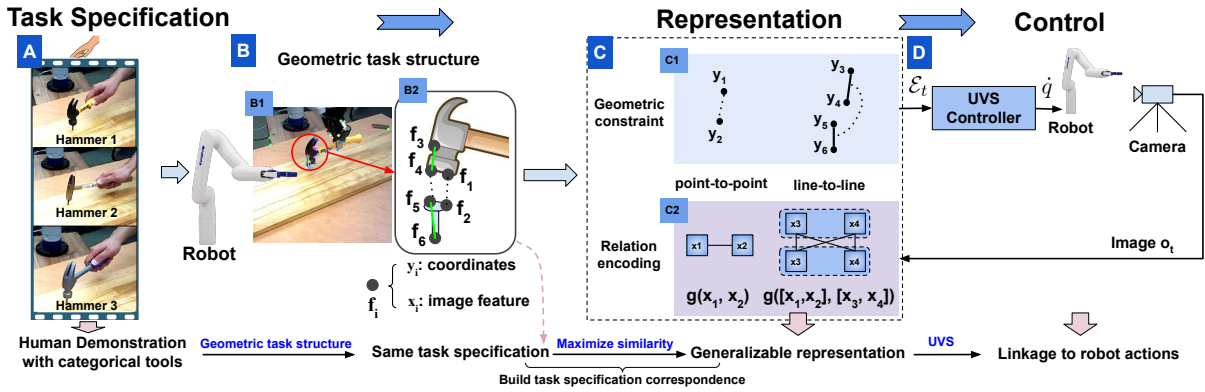


Fig. 2: Overview of our method explained using a hammering task. Given human demonstration videos (Fig. A) showing different types of hammers, we aim to learn a representation that generalizes to different hammers by introducing a geometric task structure (Fig. B) which constrains the representation space using predefined graph structures (Fig. C2), where each structure defines a geometric constraint from different hammers. Task generalization is achieved by maximizing a similarity metric between the representation of geometric constraints from different hammers. The learned representation is then mapped to robot actions (Fig. D) by its adjoint geometric error output \mathcal{E}_t that links to an uncalibrated visual servoing (UVS) controller [13]. During testing, given an image observation o_t , the learned representation selects image features to fit in the graph nodes and outputs geometric errors \mathcal{E}_t for robot control. In this example, \mathcal{E}_t is computed from the coordinate difference between two points, $[y_2 - y_1]$ and the parallelism metric between two lines, $[(y_3 \times y_4) \times (y_5 \times y_6)]$.

task by using image features on different objects. From a representation perspective, a geometric constraint is a connection relationship between geometric features (as further described in Fig. 3 and 4), which can be parameterized using relation encoders (Fig. 2 C2), such as graph neural networks (GNNs [14]) or visual transformers [15]. Thus, maximizing a similarity metric between representations of geometric constraints from different objects/tools will build the *task-specification correspondence*. This concludes the basic idea of our proposed method. To summarize, our contributions are as follows.

- We introduce a geometric task structure to learn generalizable task representations from human demonstration videos. Our proposed method learns to select task-relevant geometric constraints on categorical objects with the same task functionality to build *task specification correspondence* which enables generalization.
- We propose a novel approach to robot learning by watching human demonstrations. Our approach tackles visual imitation learning from a geometric perspective and combines it with conventional visual servoing that removes the need for extra training on the robot or pre-recorded robot motions.

We use a hammering task running on a Kinova Gen3 robot as an example with comparison to various baselines to support our contributions.

II. RELATED WORKS

A. Geometric task structure in robotics

Humans have been using points and lines to describe structural concepts for thousands of years. Many tasks in our everyday life can be described using geometric features. Likewise, in robotics, composing a task from image or point cloud data by the association, combinations and sequential linkage of geometric features is studied in the visual servo-

ing literature, including the theoretical frameworks [16–18], system [19] and applications [20].

In addition to traditional methods, geometric task structures are also used as an intermediate representation in robot learning to improve sample efficiency and task generalization. For example, S. Levine et al. 2015 [21] and their following works [22] report sample efficiency using the spatial-softmax operator to enforce the neural network extracting task-relevant feature point structures. Qin et al. 2020 [23] show task generalization in reinforcement learning by representing the task using keypoint structures.

Our work extends key point-based approaches to a more general geometry-based approach. We give a more thorough discussion on using geometric features like points, lines and conics to represent a task. Moreover, we take extra considerations on studying how to design a proper parameterization of *what* to make designing *how* much easier.

B. Generalizable visual descriptors

This paper is also inspired by the various approaches that learn generalizable visual descriptors for robotic tasks. Commonly, these approaches learn generalizable visual descriptors based on 3D correspondence, involving 3D reconstruction and then reprojecting the generated correspondence samples on the images. For example, *Dense Object Descriptor* [24], which learns a descriptor based on 3D reconstruction and image reprojection to build correspondence. Their further work kPAM [25] uses contrastive learning to explore learning dense object descriptor that is invariant across categorical objects. However, such training requires laborious annotations on each of the images.

Our work proposes to build the correspondence in an unsupervised way by extracting task-relevant geometric constraints across categorical objects. In addition to the task generalization gain in our approach, we show that using geometric constraints is more controller friendly that can

be directly applied to a geometric vision controller (visual servoing [17]). As a comparison, the above methods require tediously hand-engineered robot controllers.

III. METHOD

In this section, we firstly introduce the concept and parameterization of a geometric task structure. Then we explain how to achieve task generalization by building *task specification correspondence*. At last, we explain how to learn a generalizable task representation from human demonstration videos and map the learned representation to robot actions.

A. Geometric task structure and parameterization

Generally, an arbitrary geometric constraint is a binary relationship (Fig. 3 dashed lines) between two geometric primitives (point, line, conic and plane) observed in the image space. Considering the difficulty of representing complex geometric primitives using neural networks and that complex geometric features can be further decomposed to discrete points (Fig. 3 solid lines). A geometric constraint can be represented as a multi-entity relationship between a set of feature points $\{f_i\}$ (Fig. 3).

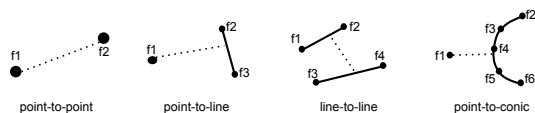


Fig. 3: An arbitrary geometric constraint is a multi-entity relationship between a set of feature points, wherein the low level, the inner-connections (solid line) between feature points $\{f_i\}$ define a complex geometric feature and in the high level, the outer-connection (dashed line) between geometric features defines different geometric constraints.

The relationship is parameterized using an undirected graph $\mathcal{G} = \{V, E\}$, with each graph node $v \in V$ representing an image feature. The connections E between graph nodes define (1) how complex geometric features are constructed from feature points (Fig. 3 solid lines); (2) how geometric features are associated as a geometric constraint (Fig. 3 dashed lines).

Using a graph to encode the relationship between image features to represent a geometric constraint was proposed in our previous work [26, 27], where the graph structure is derived by examining each possible node connection considering two properties [26]: permutation-invariant and non-inner-associative. For example, a line-to-line constraint has 38 possible node connections and the only one that fulfils the two properties is selected out (shown in Fig. 4). Details about how the graph structure is derived can be found in our supplementary material [28].

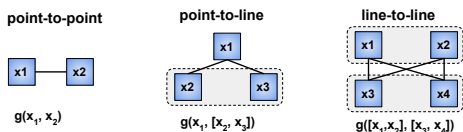


Fig. 4: The graph structure of three basic geometric constraints. The grey shaded region means the two points represent a line.

B. Task generalization by structural projection

Given a graph structure $\mathcal{G} = \{V, E\}$, where E is pre-defined to denote a geometric constraint type, projecting an image observation $o_t \in \mathbb{R}^{w \times h \times c}$ on \mathcal{G} means selecting task-relevant image features $\{f_i\}$ to fill in the graph nodes V . As shown in Fig. 1B, each image feature $\{f_i\}$ has two parts, x_i and y_i , where x_i is the feature descriptor¹ and y_i the feature’s local coordinates. Suppose a graph neural network g maps a graph \mathcal{G} instance with nodes from $\mathbf{x} = \{x_i\}$ to a latent vector $F_t \in \mathbb{R}^d$, we have,

$$\mathbf{z}_t = g(\mathbf{x}|\mathcal{G}) \quad (1)$$

Furthermore, assuming a function ϕ takes input of feature coordinates $\mathbf{y} = \{y_i\}$ and computes the related geometric constraint’s error vector \mathcal{E}_t , then,

$$\mathcal{E}_t = \psi(\mathbf{y}|\mathcal{G}) \quad (2)$$

To summarize, \mathbf{z}_t is the representation of a geometric constraint that defines the task and \mathcal{E}_t is the adjoint geometric errors that are used in a controller (such as visual servoing [17] or uncalibrated visual servoing [30]).

Then, given two arbitrary images o^i and o^j showing a task scene with two different objects i and j respectively, their task representations \mathbf{z}^i and \mathbf{z}^j build a correspondence link by maximizing a similarity metric between them since they define the same task. We use a cosine distance as the similarity metric to normalize their magnitudes:

$$\text{sim}(\mathbf{z}^i, \mathbf{z}^j) = \frac{\mathbf{z}^i \cdot \mathbf{z}^j}{\|\mathbf{z}^i\| \|\mathbf{z}^j\|} \quad (3)$$

Next, we will show that the similarity metric can be used to optimize a task function to learn generalizable task representations.

C. Task function for generalizable representation learning

In Eq. (1), a graph neural network g can read out a graph instance but can not select task-relevant features from \mathbf{x} to fill in the graph nodes. Built on top of g , a task function T_k , as introduced in [26], is designed to select task-relevant image features to construct a graph that defines the task in a geometric constraint. k denotes a geometric constraint type, such as a line-to-line constraint.

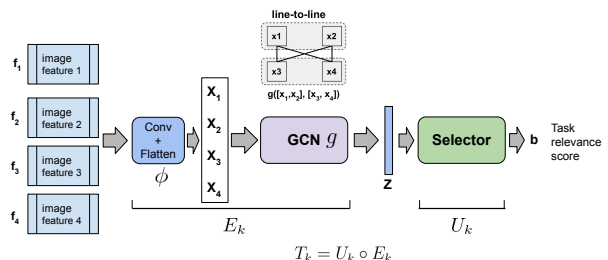


Fig. 5: Graph structured task function T_k .

A task function T_k has two parts (Fig. 5), a graph neural network-based encoder E_k that reads out a graph instance as

¹ x_i can be a hand-crafted one (such as ORB [29]) or in this paper, an image patch encoded by a convolutional neural network which is learnable.

vector \mathbf{z}_t and a selector U_k that ranks the task-relevance score of a graph instance and selects out top p graphs with high task-relevance scores. Similar to [27], we use a message-passing graph neural network [31] with GRU updates as g to encode the geometric constraints.

Learning to select task-relevant geometric constraints:

Given human demonstration videos, the above task function is optimized using VGS-IL (visual geometric skill-imitation learning [26]) by assuming the *temporal-frame-orders* in demonstrated image frame sequence that defines the task. The underlying assumption is that demonstrated image transitions encode the task definition. So that the task function is optimized to encode the task definition by maximizing the probability of observed image state transitions in the demonstrated video frames. VGS-IL enforces T_k learning to select task-relevant geometric constraints from an image. Due to page limits, readers can refer to [26] for more details.

Learning to select generalizable geometric constraints:

To make the task function T_k also select generalizable geometric constraints on different objects, we propose to combine VGS-IL with the following objective function in optimization:

$$\mathcal{L}_{sim} = \arg \max_{T_k} \frac{1}{N} \sum sim(\mathbf{z}^i, \mathbf{z}^j) \quad (4)$$

where N is the total number of image pairs from object i and j . Then by maximizing the objective function, we can enforce the task function T_k learning to select similar geometric constraints on object i and j .

D. Categorical object generalizable VGS-IL

Therefore, by joint optimization of VGS-IL [26] and the objective function in Eq. 4, we can enforce the task function T_k selecting both task-relevant and generalizable geometric constraints, thus forming a generalizable representation of the task.

Based on the above idea, we propose CoVGS-IL (Categorical object generalizable VGS-IL), which takes in a set of human demonstration videos $\mathcal{S} = \{\{o_t^i\}, \{o_t^j\}, \dots\}$ with categorical objects $\{i, j, \dots\}$ and learns a task function T_k that extracts task-relevant features on different objects with the same task functionality. In the joint optimization combining VGS-IL and the similarity loss in Eq. 4, a momentum update is applied to improve learning convergence. Algorithm details are concluded in Algorithm 1.

E. Linkage to a robot controller

The learned task function T_k is then transferred to the robot in a feedback control loop (as shown in Fig. 2D) using uncalibrated visual servoing (UVS [30]). Given an image observation o_t at time t , the task function T_k selects geometric constraints with adjoint geometric error output \mathcal{E}_t (eq. 2) that are used in an UVS controller. Examples of computing \mathcal{E}_t based on geometric constraint types are illustrated in Fig. 2.

The uncalibrated visual servoing controller (UVS [30]) uses online trial-and-error to directly estimates the Jacobian

Algorithm 1: CoVGS-IL

Input: Human demonstration videos $\mathcal{S} = \{\{o_t^i\}, \{o_t^j\}, \dots\}$ with categorical objects $\{i, j, \dots\}$; demonstrator’s confidence level α as shown in [32]; graph structural priori \mathcal{G}_k of a geometric constraint type k .

Result: Optimal weights θ^* of the task function T_k

Randomly initialize θ of T_k , cloning T_k as T_k^{sim} with weights θ_{sim}

Prepare dataset: define $\mathcal{D}_s = \{\}, \mathcal{D}_{img} = \{\}$

for each video $\{o_t^i\} \in \mathcal{S}$ **do**

Prepare state change samples \mathcal{D}^i

$\mathcal{D}_s \leftarrow$ Append \mathcal{D}^i

end

for each image frame o_t in all demo videos \mathcal{S} **do**

Extracting feature points on o_t using an off-the-shelf feature detector.

$s_t \leftarrow$ Construct all graph instances by feature association according to k

$\mathcal{D}_{img} \leftarrow$ Append s_t

end

Shuffle $\mathcal{D}, \mathcal{D}_{img}$

for $n=1:N$ **do**

Optimize T_k using the “temporal-frame-orders” loss \mathcal{L} for N_1 steps: $\theta^{n+1} = \text{VGS-IL}(\mathcal{D}, \alpha, T_k, \theta^n)$

Copy weights θ^{n+1} to θ_{sim}^n .

Optimize T_k^{sim} using the similarity loss \mathcal{L}_{sim} for N_2 steps:

$\theta_{sim}^{n+1} = \theta_{sim}^n + \nabla_{\theta_{sim}} \mathcal{L}_{sim}(\mathcal{D}_{img})$

Perform one step momentum update on T_k :

$\theta^{n+1} = \beta \theta^{n+1} + (1 - \beta) \theta_{sim}^{n+1}$, where $\beta \in (0, 1)$ is a momentum coefficient.

end

$\tilde{\mathbf{J}} \in \mathbb{R}^{d \times n}$ [13, 33] which maps image observations to robot actions, where d is the visual feature dimension, and n is the number of joints used for control. As a result, given the output geometric error signal \mathcal{E}_t at time t , the control law is formulated as:

$$\dot{\mathbf{q}} = -\lambda \tilde{\mathbf{J}}_t^+ \mathcal{E}_t \quad (5)$$

, where $\tilde{\mathbf{J}}_t^+$ is the pseudo-inverse of $\tilde{\mathbf{J}}_t$.

A UVS controller starts with an initial estimation of $\tilde{\mathbf{J}}_0$ by exploratory motions, which measure how robot action affects the numerical value changes of observed features. The initial Jacobian estimation via trial-and-errors is based on the following equation:

$$\tilde{\mathbf{J}}_0 = \left[\left[\frac{\Delta \mathbf{e}_{q_1}}{\Delta q_1} \right] \dots \left[\frac{\Delta \mathbf{e}_{q_m}}{\Delta q_m} \right] \right] \quad (6)$$

, which means the Δq_i amount of joint i movement results in geometric error change $\Delta \mathbf{e}_{q_i}$. After initial estimation, this Jacobian is then continuously updating online via Broyden update during iterations:

$$\tilde{\mathbf{J}}_{t+1} = \tilde{\mathbf{J}}_t + \alpha \frac{(\Delta \mathbf{e} - \hat{\mathbf{J}}_t \Delta q) \Delta q^T}{\Delta q^T \Delta q} \quad (7)$$

, where α is the update step size.

IV. EVALUATION

Evaluation objectives: We perform evaluations on two objectives. (1) Can CoVGS-IL learn generalizable task representations for categorical objects? (2) From an imitation

learning system perspective, can CoVGS-IL enable a real-world robot to learn generalizable skills by watching human demonstration videos?

Experimental setup: Our experimental setup is shown in Fig. 6A where an eye-to-hand camera is used to record human demonstrations and guide the robot actions. We use a hammering task (Fig. 6B and C), which requires a robot holding the hammer and hit the nail with a proper orientation². The hammer is grasped with a random pose at each run.



Fig. 6: Experimental setups. **A:** Robot-camera-demonstrator setup. **B:** Human demonstrates the hammering task from the camera’s view. **C:** Robot imitates the hammering task from the camera’s view.

From a geometric perspective, the task can be specified as a point-to-point constraint (a point on hammer bottom to a point on nail top) and line-to-line parallelism (an edge on the hammer part to the body of the nail). The learned task function is required to extract correct geometric constraints that specify the task while considering generalization to different hammers.

A. Evaluation of generalizable task representation

Training: As shown in Fig. 7, we recorded 30 human demonstration videos using three hammers (A, B and C) with ten videos for each hammer. Each video lasts about 3 to 8 seconds with about 60 to 180 frames. An ORB feature detector [29] is used to extract feature points on an image o_t . Then we run CoVGS-IL to train a graph-structured task function as described in Algorithm 1.

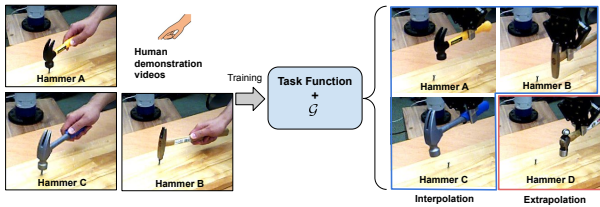


Fig. 7: Evaluating categorical object generalization regarding interpolation and extrapolation.

Evaluation protocol: Our testing strategy is to check if the learned task function will select out correct and consistent geometric constraints using five robot videos recorded by humans moving the robot with random motions, and then test the task execution performance that will be elaborated in Section IV-B.

Metrics: For video evaluation, we design two metrics. As described in [26], (1) *Acc* to measure selection accuracy by calculating the percentage of image frames with correct

²Striking motion in the final steps is not considered since it involves force/torque control which is beyond our study scope as discussed in Section V Conclusion

geometric constraint selection and (2) *ConAcc* to measure selection consistency by an auto-correlation measurement over the time-series geometric error output $\{\mathcal{E}_t\}$.

Baseline: Since there are no existing methods that learn generalizable geometric constraints from human demonstration videos, we hand-designed a *hand-tracking-baseline* based on a video-tracking module as defined in [26]. Moreover, since the *hand-tracking-baseline* does not generalize to different hammers, we manually specify the features to be tracked for each hammer. As a result, the hand-tracking baseline is a strong one since the above special considerations.

Methods	Hand-tracking		Ours		
	Acc	ConACC	Acc	ConAcc	
A	PP	100.0% ± 0.0%	1.00 ± 0.00	100.0% ± 0.0%	0.91 ± 0.05
	LL	100.0% ± 0.0%	1.00 ± 0.00	95.4% ± 3.1%	0.89 ± 0.09
B	PP	89.4% ± 8.7%	0.89 ± 0.07	88.4% ± 7.1%	0.80 ± 0.11
	LL	81.4% ± 17.7%	0.49 ± 0.59	86.2% ± 7.2%	0.60 ± 0.28
C	PP	100.0% ± 0.0%	1.00 ± 0.00	97.2% ± 3.5%	0.60 ± 0.28
	LL	96.0% ± 4.1%	0.88 ± 0.13	98.6% ± 2.3%	0.89 ± 0.08

TABLE I: Evaluation on categorical object generalization using hammer A, B and C. For convenience, “PP” refers to “point-to-point” constraint and “LL” as “line-to-line” constraint.

Categorical object generalization results: Following the above guidelines, we report the evaluation results of the task function’s performance in hammer A, B, and C. Results (Table I) show the learned task function’s performance matches the *hand-tracking* baseline.

Methods	Hand-tracking		Ours		
	Acc	ConACC	Acc	ConAcc	
D	PP	88.3% ± 8.9%	0.71 ± 0.15	91.1% ± 4.7%	0.87 ± 0.08
	LL	84.0% ± 15.1%	0.61 ± 0.42	86.7% ± 7.0%	0.74 ± 0.21

TABLE II: Categorical object generalization regarding extrapolation using hammer D.

In addition, we are also interested in testing hammer D, which is never used during training. We wonder if the learned task function will also generalize to hammer D since it shares a similar shape with hammer A and C, and a similar texture with hammer B. The testing results (Table II) surprisingly show that learned task function’s performance matches the *hand-tracking* baseline moderately. Again, note that the *hand tracking* baseline does not generalize to hammer D since it is hand designed.

Visualize task specification correspondence: Then, we visualize the select-out geometric constraints in the four types of hammers (Fig. 8). Next, we empirically evaluate if the task function learns to build *task specification correspondence* by visualizing the learned task representation for the four hammers. We visualize the output vector \mathbf{z}_t for each hammer in 16 time steps of an evaluation video. The learned task function maps a point-to-point constraint (in the form of a graph) to a representation vector \mathbf{z}_t . For simplicity, only the first element of vector \mathbf{z}_t is visualized. The color map shows how it changes along time steps (horizontal axis) and across different hammers (vertical axis).

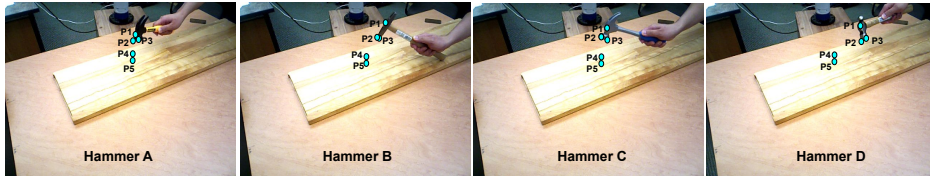


Fig. 8: Visualization of the select-out geometric constraints in the four hammers. The learned task function selects out image features (green dots) that share common characteristics among different hammers. On each hammer, the hammering task is defined by a line-to-line constraint (two lines defined by P1, P2, P4 and P5) and a point-to-point constraint (two points P3 and P4). Task specification correspondence is built by selecting the same geometric constraints (a line-to-line and a point-to-point) that define the same task.

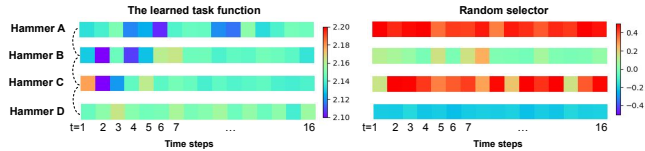


Fig. 9: Task specification correspondence visualization of the point-to-point constraint which involves two points coincidence to define the task. **Left:** the learned task function’s output z_t . **Right:** a random selector’s output z_t . A well trained task function builds the task specification correspondence by mapping graph instances of different features points on the four hammers to the same task representation z_t . It will also outputs a consistent task representation z_t along different time steps since each image frame also defines the same task using relevant geometric constraints.

We compare our method to a random selector that randomly selects a geometric constraint and input the selection to the learned task function to output a vector for visualization. Results in Fig. 9 show that the task representation z_t for hammer A, B, C and D are similar to each other while allowing slight value changes. In contrast, the random selector outputs vectors of the four hammers that do not match each other.

B. Evaluation of the imitation learning system on the robot

Lastly, we transfer the learned task function to the robot to guide the UVS controller forming a full imitation learning system.

Evaluation protocol: For hammers A, B, C and D, each hammer is evaluated using 10 robot trials with each trial changing the grasping pose. A successful trial is defined as the robot holding the hammer and hit the nail without considering knocking it down, which requires extending our method to consider force/torque control. The success rate is reported as the evaluation metric.

Baselines: We design three baselines for comparison. (1) *Behavior cloning* [6]: We collect images and robot joint reading pairs (o_t, q) for hammer A, B and C. Then, we supervised training a four-layer convolutional neural network that regresses a function mapping from image to robot joint values and uses the trained model on the robot. Each hammer has ten human demonstrations via kinesthetic teaching. (2) *Trajectory replay*: we use a pre-recorded trajectory for each hammer by human kinesthetic teaching. In testing, we replay the recorded trajectory. (3) *RL (SAC)* [34]: we train a soft-actor-critic (SAC) agent for each hammer. The policy maps image observation o_t , to the robot’s 7 joint velocities \dot{q} . Since there is no ground truth hammer pose, we use a reward classifier, similar to [35] as the reward function.

Skill generalization results: Results are shown in Table III, which indicates our method outperforms the baselines. The *behaviour cloning* baseline is hard to precisely hit the nail, which is highly dependent on the learned regressor’s accuracy. The *Trajectory replay* baseline only works for the first trial but fails during successive trials when the robot randomly grasps the hammer. The *RL (SAC)* [34] baseline failed in training after about 7 hours running on the robot.

Methods	Categorical object generalization			
	hammer A	B	C	D
Behavior cloning	20%	20%	F	F
Trajectory replay	10%	10%	10%	10%
RL (SAC)	F	F	F	F
Ours	100%	90%	100%	70%

TABLE III: Results in the hammering task considering skill generalization. “F” marks failure.

V. CONCLUSION

This paper takes a geometric perspective on the problem of generalizable task learning using human demonstration videos. Three insights enable the success of our method: (1) the insight that a geometric constraint is a multi-entity relationship between a set of image features, and the relationship can be represented using relation encoders (graph neural network in this paper); (2) the insight from visual servoing literature [17] that a wide range of robotic manipulation tasks can be specified using geometric constraints; (3) the insight that task specification is consistent under different task settings (*task specification correspondence*), which gives a clue for generalizable task representation learning.

One main limitation here is the huge computational cost required when the number of handcrafted feature points increases since the selector U_k is trained by constructing all possible graph instances that requires a combinatorial search. This limitation is more obvious when using a graph to represent complex geometric constraints like the point-to-conic. Further investigation on learning task-relevant feature detector [36] instead of a handcrafted one will solve the problem. Besides, exploring combing visual inputs with force feedbacks [37] from a geometric perspective will improve the applicability of our method in more manipulation tasks.

REFERENCES

- [1] B. C. Stadie, P. Abbeel, and I. Sutskever, “Third-person imitation learning,” *arXiv preprint arXiv:1703.01703*, 2017.
- [2] P. Sharma, D. Pathak, and A. Gupta, “Third-person visual imitation learning via decoupled hierarchical controller,” in *Advances in Neural Information Processing Systems*, 2019, pp. 2593–2603.

- [3] C. Xiong, N. Shukla, W. Xiong, and S.-C. Zhu, "Robot learning with a spatial, temporal, and causal and-or graph," in 2016 IEEE International Conference on Robotics and Automation (ICRA). IEEE, 2016, pp. 2144–2151.
- [4] D. Paulius, Y. Huang, R. Milton, W. D. Buchanan, J. Sam, and Y. Sun, "Functional object-oriented network for manipulation learning," in 2016 IEEE/RSJ International Conference on Intelligent Robots and Systems (IROS). IEEE, 2016, pp. 2655–2662.
- [5] A. Billard and R. Siegwart, "Robot learning from demonstration," Robotics and Autonomous Systems, vol. 2, no. 47, pp. 65–67, 2004.
- [6] B. D. Argall, S. Chernova, M. Veloso, and B. Browning, "A survey of robot learning from demonstration," Robotics and Autonomous Systems, vol. 57, no. 5, pp. 469–483, 2009.
- [7] A. Saxena, A. Jain, O. Sener, A. Jami, D. K. Misra, and H. S. Koppula, "Robobrain: Large-scale knowledge engine for robots," arXiv preprint arXiv:1412.0691, 2014.
- [8] D. Paulius and Y. Sun, "A survey of knowledge representation in service robotics," Robotics and Autonomous Systems, vol. 118, pp. 13–30, 2019.
- [9] Y. Yang, Y. Li, C. Fermuller, and Y. Aloimonos, "Robot learning manipulation action plans by watching unconstrained videos from the world wide web," in Twenty-Ninth AAAI Conference on Artificial Intelligence, 2015.
- [10] C. Paxton, A. Hundt, F. Jonathan, K. Guerin, and G. D. Hager, "Costar: Instructing collaborative robots with behavior trees and vision," in Robotics and Automation (ICRA), 2017 IEEE International Conference on. IEEE, 2017, pp. 564–571.
- [11] D. Leidner, C. Borst, and G. Hirzinger, "Things are made for what they are: Solving manipulation tasks by using functional object classes," in 2012 12th IEEE-RAS International Conference on Humanoid Robots (Humanoids 2012). IEEE, 2012, pp. 429–435.
- [12] F. Chaumette and S. Hutchinson, "Visual servo control. I. Basic approaches," IEEE Robotics and Automation Magazine, vol. 13, no. 4, pp. 82–90, 2006.
- [13] M. Jagersand, O. Fuentes, and R. Nelson, "Experimental evaluation of uncalibrated visual servoing for precision manipulation," Proceedings of International Conference on Robotics and Automation, vol. 4, no. April, pp. 2874–2880, 1997.
- [14] Z. Wu, S. Pan, F. Chen, G. Long, C. Zhang, and S. Y. Philip, "A comprehensive survey on graph neural networks," IEEE Transactions on Neural Networks and Learning Systems, 2020.
- [15] K. Han, Y. Wang, H. Chen, X. Chen, J. Guo, Z. Liu, Y. Tang, A. Xiao, C. Xu, Y. Xu, et al., "A survey on visual transformer," arXiv preprint arXiv:2012.12556, 2020.
- [16] G. D. Hager and Z. Dodds, "On specifying and performing visual tasks with qualitative object models," in Proceedings 2000 ICRA. Millennium Conference. IEEE International Conference on Robotics and Automation. Symposia Proceedings (Cat. No. 00CH37065), vol. 1. IEEE, 2000, pp. 636–643.
- [17] F. Chaumette, "Visual servoing using image features defined upon geometrical primitives," in Proceedings of 1994 33rd IEEE Conference on Decision and Control, vol. 4. IEEE, 1994, pp. 3782–3787.
- [18] J. P. Hespanha, Z. Dodds, G. D. Hager, and A. S. Morse, "What tasks can be performed with an uncalibrated stereo vision system?" International Journal of Computer Vision, vol. 35, no. 1, pp. 65–85, 1999.
- [19] Z. Dodds, M. Jagersand, and G. Hager, "A Hierarchical Architecture for Vision-Based Robotic Manipulation Tasks," First Int. Conf. on Computer Vision Systems, vol. 542, pp. 312–330, 1999.
- [20] M. Gridseth, O. Ramirez, C. P. Quintero, and M. Jagersand, "ViTa: Visual task specification interface for manipulation with uncalibrated visual servoing," Proceedings - IEEE International Conference on Robotics and Automation, vol. 2016-June, pp. 3434–3440, 2016.
- [21] S. Levine, C. Finn, T. Darrell, and P. Abbeel, "End-to-end training of deep visuomotor policies," The Journal of Machine Learning Research, vol. 17, no. 1, pp. 1334–1373, 2016.
- [22] C. Finn, S. Levine, and P. Abbeel, "Guided cost learning: Deep inverse optimal control via policy optimization," in International conference on machine learning, 2016, pp. 49–58.
- [23] Z. Qin, K. Fang, Y. Zhu, L. Fei-Fei, and S. Savarese, "Keto: Learning keypoint representations for tool manipulation," in 2020 IEEE International Conference on Robotics and Automation (ICRA). IEEE, 2020, pp. 7278–7285.
- [24] P. R. Florence, L. Manuelli, and R. Tedrake, "Dense object nets: Learning dense visual object descriptors by and for robotic manipulation," arXiv preprint arXiv:1806.08756, 2018.
- [25] L. Manuelli, W. Gao, P. Florence, and R. Tedrake, "kpm: Keypoint affordances for category-level robotic manipulation," arXiv preprint arXiv:1903.06684, 2019.
- [26] J. Jin, L. Petrich, M. Dehghan, and M. Jagersand, "A geometric perspective on visual imitation learning," in 2020 IEEE/RSJ International Conference on Intelligent Robots and Systems (IROS). IEEE, 2020, pp. 2655–2662.
- [27] J. Jin, L. Petrich, Z. Zhang, M. Dehghan, and M. Jagersand, "Visual geometric skill inference by watching human demonstration," in 2020 IEEE International Conference on Robotics and Automation (ICRA). IEEE, 2020, pp. 8985–8991.
- [28] Jin, Jun and Jagersand, Martin, "Supplementary materials for generalizable task representation learning from human demonstration videos: a geometric approach," 2021, [Online; accessed 14-Sept-2021]. [Online]. Available: <http://webdocs.cs.ualberta.ca/~vis/Jun/CoVGS-IL/supplementary-material.pdf>
- [29] E. Rublee, V. Rabaud, K. Konolige, and G. R. Bradski, "Orb: An efficient alternative to sift or surf," in ICCV, vol. 11, no. 1. Citeseer, 2011, p. 2.
- [30] M. Jagersand and R. Nelson, "Visual space task specification, planning and control," in Proceedings of International Symposium on Computer Vision-ISCV. IEEE, 1995, pp. 521–526.
- [31] J. Gilmer, S. S. Schoenholz, P. F. Riley, O. Vinyals, and G. E. Dahl, "Neural message passing for quantum chemistry," in Proceedings of the 34th International Conference on Machine Learning-Volume 70. JMLR.org, 2017, pp. 1263–1272.
- [32] J. Jin, L. Petrich, M. Dehghan, Z. Zhang, and M. Jagersand, "Robot eye-hand coordination learning by watching human demonstrations: a task function approximation approach," in 2019 International Conference on Robotics and Automation (ICRA). IEEE, 2019, pp. 6624–6630.
- [33] O. A. Ramirez and M. Jagersand, "Practical considerations of uncalibrated visual servoing," Proceedings - 2016 13th Conference on Computer and Robot Vision, CRV 2016, pp. 164–169, 2016.
- [34] T. Haarnoja, A. Zhou, P. Abbeel, and S. Levine, "Soft actor-critic: Off-policy maximum entropy deep reinforcement learning with a stochastic actor," in International conference on machine learning. PMLR, 2018, pp. 1861–1870.
- [35] G. Dulac-Arnold, D. Mankowitz, and T. Hester, "Challenges of real-world reinforcement learning," arXiv preprint arXiv:1904.12901, 2019.
- [36] T. Kulkarni, A. Gupta, C. Ionescu, S. Borgeaud, M. Reynolds, A. Zisserman, and V. Mnih, "Unsupervised learning of object keypoints for perception and control," arXiv preprint arXiv:1906.11883, 2019.
- [37] J. Jin, D. Graves, C. Haigh, J. Luo, and M. Jagersand, "Offline learning of counterfactual perception as prediction for real-world robotic reinforcement learning," arXiv preprint arXiv:2011.05857, 2020.